POLITECNICO DI TORINO
Repository ISTITUZIONALE

High-Fidelity Imaging of the Brain’s Electrophysiological Activity Based on a Fast Direct Solver

Original
High-Fidelity Imaging of the Brain’s Electrophysiological Activity Based on a Fast Direct Solver / Merlini, A., Giunzioni, V., Henry, C., Adrian, S.B., Andriulli, F.P.. - (2025). (URSI AP-RASC, Sydney, Australia, 17 – 22 August 2025 Sydney (Aus) 17 – 22 August 2025) [10.46620/URSIAPRASC25/CFCS2383].

Availability:
This version is available at: 11583/3006318 since: 2026-01-07T16:38:04Z

Publisher:
URSI

Published
DOI:10.46620/URSIAPRASC25/CFCS2383

Terms of use:

This article is made available under terms and conditions as specified in the corresponding bibliographic description in the repository

Publisher copyright

(Article begins on next page)

26 June 2026

URSI AP-RASC, Sydney, Australia, 17 – 22 August 2025

High-Fidelity Imaging of the Brain's Electrophysiological Activity Based on a Fast Direct Solver

Adrien Merlini*(1), Viviana Giunzioni(2), Clément Henry(1), Simon B. Adrian(3), and Francesco P. Andriulli(2)
(1) IMT Atlantique, Brest, France
(2) Politecnico di Torino, Torino, Italy
(3) Universität Rostock, Rostock, Germany

Abstract

Imaging of the electrophysiologic activity of the brain is important for diagnosing or treating several neurological diseases. Electroencephalography source imaging (ESI) is a modality that reconstructs the electrophysiologic activity from external potential measurement at the scalp. Despite being non-invasive and being capable of offering high temporal and spatial resolutions, its adoption is hampered by its complexity and high computational cost caused by its need to solve a complex forward problem from hundreds to thousands of times per subject. In this contribution, we tackle this issue by presenting a fast direct solver for ESI that yields a low-rank skeleton form of the inverse of the forward problem, allowing for a drastic reduction in the computational load of the imaging modality.

1. Introduction

Several neurological disorders such as Parkinson's disease and focal epilepsy require precise diagnostic approaches that can map brain electrical dynamics. Minimally invasive neuroimaging techniques such as electroencephalography (EEG) source imaging (ESI) leverage external head measurements to reconstruct intracranial electrical patterns. The fundamental challenge in these approaches lies in accurately modeling how the electrical currents generated by the neurons propagate through the complex head anatomy. This process involves solving the forward EEG problem to accurately capture the propagation and distribution of bioelectrical signals through heterogeneous head tissues, and the accuracy of the imaging is intrinsically tied to the accuracy with which the forward problem can be solved.

Enhancing the precision of forward modeling requires attacking the problem from different angles. The first approach centers on obtaining detailed anatomical and physiological characteristics of the head through cutting-edge anatomic imaging technologies, particularly magnetic resonance imaging (MRI). Subsequently a numerical approach to simulate electrical behavior within the head's complex structure must be carefully selected. While multiple computational methods exist, boundary element methods (BEM) emerge as particularly attractive due to their computational efficiency and ability to place unknowns exclusively at tissue interfaces. Within the realm of BEM head modeling, the symmetric formulation is one of the most attractive due to its high accuracy [1]. However, this approach suffers from several sources of numerical instability that hinders its applicability to the most complex scenarii, especially when dealing with fine-grained discretizations and substantial tissue conductivity contrasts. These fundamental limitations dramatically restrict the potential for developing high-resolution head models. In addition, the high computational load required to accurately model forward problems also limits the level of accuracy that can be achieved. The large dimensions of the linear systems to be inverted for solving the forward problem make direct system inversion impractical—or prevent it altogether. As a result, each solution of the forward problem will require invoking an iterative solver. This becomes especially challenging in brain imaging contexts, where the forward problem needs to be solved hundreds to thousands of times, depending of the required accuracy of reconstructed electrical activity maps. The cumulative computational demands quickly become prohibitive, an effect that is compounded by the fact that iterative solvers experience slower convergence and reduced numerical stability for mathematically ill-conditioned systems, such as those arising from the BEM discretization of the symmetric formulation [2].

In this work, we present a new fast direct solver strategy allowing for significantly reduced complexity in the computation of the ESI models. This fast direct solver first leverages a recently introduced preconditioner based on a Calderón-like approach [2]. This preconditioned formulation cures the dense discretization and high-contrast numerical instabilities of the original equation. Building upon this foundation, we transform the system's spectral characteristics using newly developed quasi-Helmholtz filters [3]. This spectral manipulation enhances the compressibility of the system matrices, which can then be used to directly compress the inverse of these spectrally-modified systems into efficient skeleton representations. Finally, using Woodbury matrix identities [4], we subsequently construct a non-hierarchical fast direct solver specifically optimized for electroencephalography brain imaging applications. The methodology's computational performance and theoretical robustness will be demonstrated through numerical experiments that highlight practical relevance and computational efficiency.

2. Background and Notations

In the EEG forward problem, we aim at recovering the potential V at the electrodes generated by the primary brain activity (current) $\boldsymbol{j}$. This amounts to solving Poisson's equation $\nabla \cdot (\sigma \nabla V) = \nabla \cdot \boldsymbol{j}$ [5], in a nested domain $\Omega = \cup_{i=1}^{N} \Omega_i$ with boundaries $\Gamma_i = \overline{\Omega}_i \cap \overline{\Omega}_{i+1}$ with outgoing normals $\boldsymbol{n}_i$, and a constant conductivity σ_i in Ω_i. The representation theorem produces $2N$ equations [1]

$$(\partial_{\boldsymbol{n}} v_{i+1})_{\Gamma_i} - (\partial_{\boldsymbol{n}} v_i)_{\Gamma_i} = -\mathcal{D}^*_{i,i-1} p_{i-1} + 2\mathcal{D}^*_{ii} p_i - \mathcal{D}^*_{i,i+1} p_{i+1} + \sigma_i \mathcal{N}_{i,i-1} V_{i-1} - (\sigma_i + \sigma_{i+1}) \mathcal{N}_{ii} V_i + \sigma_{i+1} \mathcal{N}_{i,i+1} V_{i+1} \quad (1)$$

$$\sigma_{i+1}^{-1} (v_{i+1})_{\Gamma_i} - \sigma_i^{-1} (v_i)_{\Gamma_i} = \mathcal{D}_{i,i-1} V_{i-1} - 2\mathcal{D}_{ii} V_i + \mathcal{D}_{i,i+1} V_{i+1} - \sigma_i^{-1} \mathcal{S}_{i,i-1} p_{i-1} + (\sigma_i^{-1} + \sigma_{i+1}^{-1}) \mathcal{S}_{ii} p_i - \sigma_{i+1}^{-1} \mathcal{S}_{i,i+1} p_{i+1}, \quad (2)$$

where $V_i = (V)_{\Gamma_i}$, $p_i = \sigma_i [\boldsymbol{n}_i \cdot \nabla V]_{\Gamma_i}$, $v_i = f_i * G$, $f_i = \nabla \cdot \boldsymbol{j}$ in Ω_i and 0 elsewhere, and $G(\boldsymbol{r}, \boldsymbol{r}') = 1/(4\pi|\boldsymbol{r} - \boldsymbol{r}'|)$. The operators are the standard scalar operators $(\mathcal{S}\psi)(\boldsymbol{r}) = \int_{\partial\Omega} G(\boldsymbol{r}, \boldsymbol{r}') \psi(\boldsymbol{r}') \mathrm{d}S(\boldsymbol{r}')$, $\mathcal{D}\phi(\boldsymbol{r}) = \text{p.v.} \int_{\partial\Omega} \partial_{\boldsymbol{n}'} G(\boldsymbol{r}, \boldsymbol{r}') \phi(\boldsymbol{r}') \mathrm{d}S(\boldsymbol{r}')$, $\mathcal{D}^*\psi(\boldsymbol{r}) = \text{p.v.} \int_{\partial\Omega} \partial_{\boldsymbol{n}} G(\boldsymbol{r}, \boldsymbol{r}') \psi(\boldsymbol{r}') \mathrm{d}S(\boldsymbol{r}')$, and $\mathcal{N}\phi(\boldsymbol{r}) = \int_{\partial\Omega} \partial_{\boldsymbol{n}} \partial_{\boldsymbol{n}'} G(\boldsymbol{r}, \boldsymbol{r}') \phi(\boldsymbol{r}') \mathrm{d}S(\boldsymbol{r}')$. Here, $_{ij}$ is the restriction to $\boldsymbol{r} \in \Gamma_i$ and $\boldsymbol{r}' \in \Gamma_j$. To solve this system numerically, a mesh with N_c cells and N_v vertices is created. The basis functions are the piecewise constant functions $\{\pi_n\}_{n=1}^{N_\mathrm{c}}$ and piecewise linear functions $\{\lambda_n\}_{n=1}^{N_\mathrm{v}}$. The unknowns are expanded as $V_i = \sum_{n=1}^{N_\mathrm{v}} v_{i,n} \lambda_n$, $p_i = \sum_{n=1}^{N_\mathrm{c}} p_{i,n} \pi_n$ and the new equations are tested with the appropriate functions λ and π. When $N = 1$, the system to be solved is $\boldsymbol{Z}[\boldsymbol{v}^\mathrm{T}\ \boldsymbol{p}^\mathrm{T}]^\mathrm{T} = [\boldsymbol{b}^\mathrm{T}\ \boldsymbol{c}^\mathrm{T}]^\mathrm{T}$, with $\boldsymbol{Z} = \left[\boldsymbol{N}\ \boldsymbol{D}^*; \boldsymbol{D}\ \boldsymbol{S}\right]$, $[\boldsymbol{N}]_{mn} = (\sigma_1 + \sigma_2)(\lambda_m, \mathcal{N}_{11}\lambda_n)_{L^2(\Gamma_1)}$, $[\boldsymbol{D}^*]_{mn} = -2\left(\lambda_m, \mathcal{D}^*_{11}\pi_n\right)_{L^2(\Gamma_1)}$, $[\boldsymbol{D}]_{mn} = -2(\pi_m, \mathcal{D}_{11}\lambda_n)_{L^2(\Gamma_1)}$, $[\boldsymbol{S}]_{mn} = (\sigma_1^{-1} + \sigma_2^{-1})(\pi_m, \mathcal{S}_{11}\pi_n)_{L^2(\Gamma_1)}$, $[\boldsymbol{v}]_m = v_{1,m}$, $[\boldsymbol{p}]_m = p_{1,m}$, $[\boldsymbol{b}]_m = -(\lambda_m, \partial_{\boldsymbol{n}} v_1)_{L^2(\Gamma_1)}$, and $[\boldsymbol{c}]_m = -\sigma_1^{-1}(\pi_m, v_1)_{L^2(\Gamma_1)}$.

The system is then preconditioned as delineated in [2]

$$\tilde{\boldsymbol{Z}} \boldsymbol{G}^{-1} \boldsymbol{Z}\ \boldsymbol{y} = \tilde{\boldsymbol{Z}} \boldsymbol{G}^{-1} \left[\boldsymbol{b}^\mathrm{T} \quad \boldsymbol{c}^\mathrm{T}\right]^\mathrm{T}. \quad (3)$$

where $\boldsymbol{G} = \mathrm{diag}(\boldsymbol{G}_{\tilde{\pi}\lambda}, \boldsymbol{G}_{\tilde{\lambda}\pi})$, with $\boldsymbol{G}_{\tilde{\pi}\lambda}$ and $\boldsymbol{G}_{\tilde{\lambda}\pi}$ the mixed Gram matrices between dual patches and pyramids and dual pyramids and patches, respectively. The matrix $\tilde{\boldsymbol{Z}}$ is defined from the dual discretization as $\boldsymbol{Z} = \left[\tilde{\boldsymbol{S}}\ \tilde{\boldsymbol{D}}; \tilde{\boldsymbol{D}}^*\ \tilde{\boldsymbol{N}}\right]$ with $\left[\tilde{\boldsymbol{S}}\right]_{mn} = (\sigma_1 + \sigma_2)(\tilde{\pi}_m, \mathcal{S}_{11}\tilde{\pi}_n)_{L^2(\Gamma_1)}$, $\left[\tilde{\boldsymbol{D}}^*\right]_{mn} = -2\left(\tilde{\lambda}_m, \mathcal{D}^*_{11}\tilde{\pi}_n\right)_{L^2(\Gamma_1)}$, $\left[\tilde{\boldsymbol{D}}\right]_{mn} = -2\left(\tilde{\pi}_m, \mathcal{D}_{11}\tilde{\lambda}_n\right)_{L^2(\Gamma_1)}$, $\left[\tilde{\boldsymbol{N}}\right]_{mn} = (\sigma_1^{-1} + \sigma_2^{-1})\left(\tilde{\lambda}_m, \mathcal{N}_{11}\tilde{\lambda}_n\right)_{L^2(\Gamma_1)}$. Note that for clarity, the high contrast preconditioning has been omitted, but this will not change the core results of the paper.

3. A New Fast Direct Solver

In the following we leverage results regarding the second-kind and compact nature of the blocks of $\tilde{\boldsymbol{Z}} \boldsymbol{G}^{-1} \boldsymbol{Z}$ that, to facilitate the discussion, we express as

$$\tilde{\boldsymbol{Z}} \boldsymbol{G}^{-1} \boldsymbol{Z} = \begin{bmatrix} \alpha_{11}\boldsymbol{I}_{11} + \boldsymbol{C}_{11} & \boldsymbol{C}_{12} \\ \boldsymbol{C}_{21} & \alpha_{22}\boldsymbol{I}_{22} + \boldsymbol{C}_{22} \end{bmatrix} \quad (4)$$

where the matrices $\boldsymbol{I}_{ii}$ stand for matrices with a spectrum converging to a non-zero value, and $\boldsymbol{C}_{ij}$ matrices with a spectrum clustering to 0. Formally, these filtering matrices require the usage of square roots of Gram matrices, that are omitted here for readability. Lamentably, these spectral properties cannot be exploited directly and $\tilde{\boldsymbol{Z}} \boldsymbol{G}^{-1} \boldsymbol{Z} - \mathrm{diag}(\alpha_{11}\boldsymbol{I}_{11}, \alpha_{22}\boldsymbol{I}_{22})$ cannot be compressed directly without resorting to a computationally expensive and complex hierarchical scheme. To address this issue we leverage the recently introduced quasi-Helmholtz filters in the form of filtered Laplacian matrices $(\boldsymbol{\Delta})_m$ and $(\tilde{\boldsymbol{\Delta}})_m$, with $[\boldsymbol{\Delta}]_{mn} = (\nabla\lambda_m, \nabla\lambda_n)_{L^2(\Gamma_1)}$, $[\tilde{\boldsymbol{\Delta}}]_{mn} = \left(\nabla\tilde{\lambda}_m, \nabla\tilde{\lambda}_n\right)_{L^2(\Gamma_1)}$, and the notation $(\boldsymbol{X})_m$ indicates that the symmetric matrix $\boldsymbol{X} \in \mathbb{R}^{n\times n}$ has been spectrally filtered, i.e., given its singular value decomposition $\boldsymbol{X} = \boldsymbol{U}\,\mathrm{diag}(s_1, \ldots, s_m, \ldots, s_n)\,\boldsymbol{V}^\mathrm{T}$, $(\boldsymbol{X})_m = \boldsymbol{U}\,\mathrm{diag}(s_1, \ldots, s_m, 0, \ldots, 0)\,\boldsymbol{V}^\mathrm{T}$, where $\{s_i\}_{i=1}^n$ are the singular values of $\boldsymbol{X}$. These filtered matrices, that can be built fast—without invoking the SVD—using the techniques presented in [3] thanks to the properties of the Laplacian matrices, will be used as to form a filtering matrix $\boldsymbol{F} = \mathrm{diag}((\boldsymbol{\Delta})_m, (\tilde{\boldsymbol{\Delta}})_m)$ to filter the compact part of the preconditioned symmetric formulation matrix as

$$\boldsymbol{F}\left(\tilde{\boldsymbol{Z}} \boldsymbol{G}^{-1} \boldsymbol{Z} - \begin{bmatrix} \alpha_{11}\boldsymbol{I}_{11} & \boldsymbol{0} \\ \boldsymbol{0} & \alpha_{22}\boldsymbol{I}_{22} \end{bmatrix}\right) = \begin{bmatrix} (\boldsymbol{\Delta})_m \boldsymbol{C}_{11} & (\boldsymbol{\Delta})_m \boldsymbol{C}_{12} \\ (\tilde{\boldsymbol{\Delta}})_m \boldsymbol{C}_{21} & (\tilde{\boldsymbol{\Delta}})_m \boldsymbol{C}_{22} \end{bmatrix}. \quad (5)$$

Thanks to the compression-enhancing properties of the Laplacian filters, the blocks of the form $(\boldsymbol{\Delta})_m \boldsymbol{C}_{ij}$ and $(\tilde{\boldsymbol{\Delta}})_m \boldsymbol{C}_{ij}$ can now be compressed using standard, non-hierarchical compression algorithm such as the adaptive cross approximation [6] or randomized schemes. In practice, this means that we can compute, for each of these filtered blocks, a skeleton form $\boldsymbol{U}_{ij}\boldsymbol{V}_{ij}^\mathrm{T}$ such that $(\boldsymbol{\Delta})_m \boldsymbol{C}_{ij} = \boldsymbol{U}_{ij}\boldsymbol{V}_{ij}^\mathrm{T} + \boldsymbol{E}_{ij}$, where $(\boldsymbol{U}, \boldsymbol{V}) \in (\mathbb{R}^{N\times r})^2$. The rank r of the skeleton form depends on the accuracy required and will impact the norm of the compression error $\|\boldsymbol{E}_{ij}\|$. For properly chosen operators, this rank r will be independent of the discretization. This compression results in an overall system in semi-compressed form

$$\tilde{\boldsymbol{Z}} \boldsymbol{G}^{-1} \boldsymbol{Z} \approx: \boldsymbol{M} = \begin{bmatrix} \alpha_{11}\boldsymbol{I}_{11} + \boldsymbol{U}_{11}\boldsymbol{V}_{11}^\mathrm{T} & \boldsymbol{U}_{12}\boldsymbol{V}_{12}^\mathrm{T} \\ \boldsymbol{U}_{21}\boldsymbol{V}_{21}^\mathrm{T} & \alpha_{22}\boldsymbol{I}_{22} + \boldsymbol{U}_{22}\boldsymbol{V}_{22}^\mathrm{T} \end{bmatrix}. \quad (6)$$

The last step to form a fast direct solver is to construct a compressed representation of $\boldsymbol{M}^{-1}$, which can be achived by leveraging the block matrix identities [4] and the low rank approximations of the blocks of $\tilde{\boldsymbol{M}}$. For instance, if we denote

$\tilde{M}^{-1} =: \left[A_{11}\, A_{12}; A_{21}\, A_{22}\right]$, we have

$$A_{11} = \Big(\alpha_{11} I_{11} + U_{11} V_{11}^{\mathrm{T}} - U_{12} V_{12}^{T} \left(\alpha_{22} I_{22} + U_{22} V_{22}^{\mathrm{T}}\right)^{-1} U_{21} V_{21}^{T}\Big)^{-1} . \quad (7)$$

By carefully inspecting the dimensions of the matrices involved in the computation, we notice that we can compute a skeleton form for A_{11} using the skeleton forms of the blocks of $\tilde{Z}$ and we rewrite the block of the inverse as

$$A_{11} = \left(\alpha_{11} I_{11} + \tilde{U}_{11} \tilde{V}_{11}^{\mathrm{T}}\right)^{-1} \quad (8)$$

for which we have a fast matrix vector product using the Woodbury matrix identity [4]

$$A_{11} x = \alpha_{11}^{-1} I_{11} x + \alpha_{11}^{-2} \tilde{U}_{11} \left(I_r + \alpha_{11}^{-1} \tilde{V}_{11}^{\mathrm{T}} \tilde{U}_{11}\right)^{-1} \tilde{V}_{11}^{\mathrm{T}} x . \quad (9)$$

Note that the dimension of the inner matrix to be inverted is the rank of the corresponding block of the original system matrix, as such the computational cost of this inversion is constant if r is independent of the dimension of the original system. A similar procedure can be applied to all the block A_{ij}, which in turn means that the matrix M^{-1} can multiplied fast to any vector $\left[b; c\right]$ as

$$M^{-1} \begin{bmatrix} b \\ c \end{bmatrix} = \begin{bmatrix} A_{11} b + A_{12} c \\ A_{21} b + A_{22} c \end{bmatrix} , \quad (10)$$

and this representation of M^{-1} is indeed a fast direct solver for the EEG forward problem, that does not require any hierarchical decomposition to be constructed.

4. Numerical Results

To numerically validate our scheme, we consider the case of a single compartment head to maintain consistency with the derivation of the Section 3, but these considerations can be extended to higher numbers of nested compartments. In Figure 1 we compare the accuracy of the solution of the fast direct solver by comparing it against a traditional direct inversion; the error introduced by the compression decreases with discretization until it saturates at a fixed value close to the compression threshold we have selected. This figure also reports the rank of the skeleton forms of A_{11} and A_{22} for increasing discretization that remains constant for increasing discretization, thus validating the low computational complexity of the scheme.

Finally, we verify that the scheme can be applied to more challenging cases with a one compartment head model extracted from an MRI. The top picture in Figure 2 shows the potential generated on the scalp by a singular current dipole placed inside the head to model neuronal activity, computed using the fast direct solver. The bottom picture shows the corresponding absolute error between the fast direct solver solution and the standard solution obtained via direct matrix inversion with a good agreement between the two solutions.

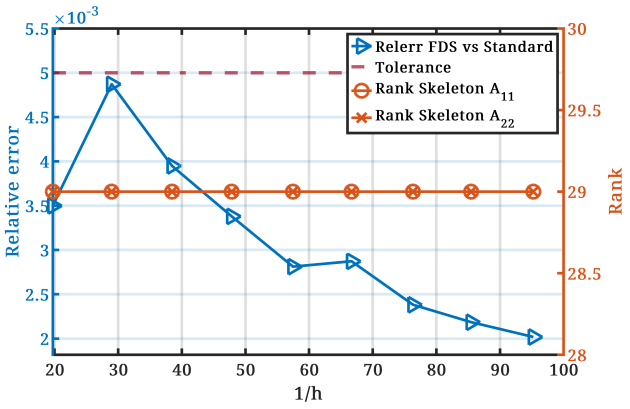

Figure 1: Relative error between the solution of the fast direct solver and the solution obtained by direct matrix inversion and rank of the blocks A_{11} and A_{22}. The results correspond to a single compartment sphere with radius 0.087 m, normalized conductivity $\sigma_1 = 1$ and background normalized conductivity $\sigma_2 = 1/80$, a target accuracy for the adaptive cross approximations of 5×10^{-3}, and a filtering index $m = 30$.

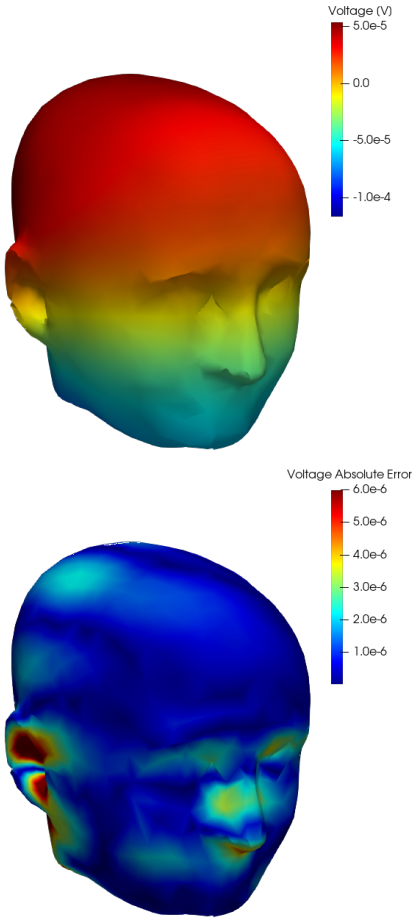

Figure 2: Potential generated on the scalp by a dipolar current source inside the head, computed with the fast direct solver along with the absolute error between the fast direct solver and standard solution.

5. Acknowledgements

This work was supported by the European Innovation Council (EIC) through the European Union's Horizon Europe research Programme under Grant 101046748 (Project CEREBRO) and has received a French government support granted to the Labex CominLabs excellence laboratory and managed by the National Research Agency in the "Investing for the Future" program under reference ANR-10-LABX-07-01.

References

[1] J. Kybic, M. Clerc, T. Abboud, O. Faugeras, R. Keriven, and T. Papadopoulo, "A common formalism for the Integral formulations of the forward EEG problem," *IEEE Transactions on Medical Imaging*, vol. 24, no. 1, pp. 12–28, Jan. 2005, ISSN: 0278-0062. DOI: 10.1109/TMI.2004.837363.

[2] J. E. Ortiz G., A. Pillain, L. Rahmouni, and F. P. Andriulli, "A Calderon regularized symmetric formulation for the electroencephalography forward problem," *Journal of Computational Physics*, vol. 375, pp. 291–306, Dec. 15, 2018, ISSN: 0021-9991. DOI: 10.1016/j.jcp.2018.07.048.

[3] A. Merlini, C. Henry, D. Consoli, L. Rahmouni, A. Dély, and F. P. Andriulli, "Laplacian Filtered Loop-Star Decompositions and Quasi-Helmholtz Filters: Definitions, Analysis, and Efficient Algorithms," *IEEE Transactions on Antennas and Propagation*, pp. 1–1, 2023, ISSN: 0018-926X, 1558-2221. DOI: 10.1109/TAP.2023.3283043.

[4] H. V. Henderson and S. R. Searle, "On Deriving the Inverse of a Sum of Matrices," *SIAM Review*, vol. 23, no. 1, pp. 53–60, Jan. 1981, ISSN: 0036-1445, 1095-7200. DOI: 10.1137/1023004.

[5] M. Darbas and S. Lohrengel, "Review on Mathematical Modelling of Electroencephalography (EEG)," *Jahresbericht der Deutschen Mathematiker-Vereinigung*, vol. 121, no. 1, pp. 3–39, Mar. 1, 2019, ISSN: 1869-7135. DOI: 10.1365/s13291-018-0183-z.

[6] M. Bebendorf, "Approximation of boundary element matrices," *Numerische Mathematik*, vol. 86, no. 4, pp. 565–589, 2000.